Journal of Hazardous Materials 194 (2011) 312–323

Contents lists available at ScienceDirect

Journal of Hazardous Materials

journal homepage: www.elsevier.com/locate/jhazmat

Removal of cadmium, copper, nickel, cobalt and mercury from water by Apatite II™: Column experiments

Josep Oliva [a], Joan De Pablo [b], José-Luis Cortina [b,c,*], Jordi Cama [d], Carlos Ayora [d]

[a] Department of Mining Engineering and Natural Resou-rces, Universitat Politècnica de Catalunya, Bases de Manresa 61-73, 08242 Manresa, Catalonia, Spain
[b] Department of Chemical Engineering, Universitat Politècnica de Catalunya, Diagonal 647, 08028 Barcelona, Catalonia, Spain
[c] Water Technology Center, CETaqua, Paseo de los Tilos 3, 08034 Barcelona, Catalonia, Spain
[d] Institute of Environmental Assessment and Water Research, IDAEA, CSIC, Jordi Girona 18, 08034 Barcelona, Catalonia, Spain

ARTICLE INFO

Article history:
Received 25 February 2011
Received in revised form 25 July 2011
Accepted 28 July 2011
Available online 7 August 2011

Keywords:
Passive treatment
Hydroxyapatite
Phosphate
Heavy metal
Immobilisation

ABSTRACT

Apatite II™, a biogenic hydroxyapatite, was evaluated as a reactive material for heavy metal (Cd, Cu, Co, Ni and Hg) removal in passive treatments. Apatite II™ reacts with acid water by releasing phosphates that increase the pH up to 6.5–7.5, complexing and *inducing metals to precipitate as metal phosphates*. The evolution of the solution concentration of calcium, phosphate and metals together with SEM–EDS and XRD examinations were used to identify the retention mechanisms. SEM observation shows low-crystalline precipitate layers composed of P, O and M. Only in the case of Hg and Co were small amounts of crystalline phases detected. Solubility data values were used to predict the measured column experiment values and to support the removal process based on the dissolution of hydroxyapatite, the formation of metal–phosphate species in solution and the precipitation of metal phosphate. $Cd_5(PO_4)_3OH(s)$, $Cu_2(PO_4)OH(s)$, $Ni_3(PO_4)_2(s)$, $Co_3(PO_4)_2 8H_2O(s)$ and $Hg_3(PO_4)_2(s)$ are proposed as the possible mineral phases responsible for the removal processes. The results of the column experiments show that Apatite II™ is a suitable filling for permeable reactive barriers.

1. Introduction

Polymetallic sulphides (Fe, Mn, Cu, Cd, Zn, Ni, Co, Hg) are one of the main sources of contaminated water in abandoned mines and waste dumps [1,2]. The release of these metals into bodies of water is increasing, and non-admissible levels are found in surface and groundwaters. Given their properties as active carcinogenic agents, only a maximum admissible concentration of 20 μg/L for Ni, 1 μg/L for Hg and 5 μg/L for Cd is permitted [3,4]. The toxicity of Co is usually lower but can be high in the case of radioactive wastes in conjunction with Ni. The US Environmental Protection Agency (USEPA) prepared a list of 129 organic and inorganic pollutants found in wastewater that constitute serious health hazards. This Priority Pollutants List includes thirteen elements: Sb, As, Be, Cd, Cr, Cu, Pb, Hg, Ni, Se, Ag, Tl and Zn.

Passive remediation systems such as permeable reactive barriers (PRBs) are a good alternative to remediate contaminated groundwater [5]. PRBs are a passive technology that installs a reactive material across the migration path of a contaminated aquifer. Groundwater flows through and reacts with the material at the barrier, causing the acidity of the water to be neutralised and the metals retained. PRB materials are effective provided they meet the following conditions [6]: (1) they are sufficiently reactive to diminish the concentrations of the pollutants within the residence time for the water inside the PRB; (2) they are permeable enough to concentrate the flow of the groundwater; (3) they preserve the permeability and reactivity for long duration; and (4) they are cost effective. Conventional proposals for reactive materials to treat metal contamination such as calcite result in the removal of trivalent metals (Fe, Al) by increasing the pH up to a value of 6–7. The efficient removal of divalent metals, however, requires increasing the pH to higher values [7,8]. Magnesium oxide has been shown to increase the pH up to 8–9 and to promote the high removal efficiency of divalent metals such as Cu, Zn, Pb, Mn, Ni, Co and Cd [9]. An alternative to the use of magnesium oxide for the retention of divalent metals is represented by the application of phosphate amendments.

Among the different sources of phosphate, both natural and synthetic hydroxyapatite (HAP) has been postulated as a reactive material to remove metals [10,11]. Natural HAP has been demonstrated to immobilise Pb, Zn and U [12–15]. A synthetic phosphate has a much larger surface area and has been used in nanotechnology applications as well as in water and soil metal decontamination [16–19]. Most synthetic compounds, however, are too expensive for the extensive applications in infiltration ponds and reactive barriers.

* Corresponding author at: Department of Chemical Engineering, Universitat Politècnica de Catalunya, Diagonal 647, 08028 Barcelona, Catalonia, Spain.
E-mail address: jose.luis.cortina@upc.edu (J.-L. Cortina).

0304-3894/$ – see front matter © 2011 Elsevier B.V. All rights reserved.
doi:10.1016/j.jhazmat.2011.07.104

Table 1
Initial condition in the column experiments.

Experiments						
	Column					
	0	1	2	3	4	5
Length (mm)	17.44	18.60	17.44	16.86	16.28	31.97
Section (mm^2)	172.03	172.03	172.03	172.03	172.03	172.03
Volume (mL)	3	3.2	3	2.9	2.8	5.5
Sample (g)						
Initial	2.492	2.512	2.576	2.517	2.560	2.513
Final	1.102	2.985	2.481	2.042	2.343	0.804
Particle size (mm)	0.5–3	0.5–3	0.5–3	0.5–3	0.5–3	0.5–3
Apatite II^{TM} (wt.%)	100	100	100	100	100	100
Pore vol (mL)	1.5	1.7	1.4	1.3	1.2	2.6
Porosity	0.49	0.52	0.47	0.46	0.44	0.48
BET surface areas ($m^2\ g^{-1}$)						
Initial	1.9	1.9	1.9	1.9	1.9	1.9
Final	100	47.3	41.8	24.8	17.1	1
Flow (mL/min)	0.02	0.02	0.02	0.02	0.02	0.02
Residence time (min)	73	83	71	67	61	132
Inlet						
pH	4.5	4.9	4.8	5.0	5.0	2.0
Cd (mM)		0.67				
Cu (mM)			1.18			
Ni (mM)				1.28		
Co (mM)					1.27	
Hg (mM)						0.37
SO_4^{2-} (mM)	10.41	10.41	10.41	10.41	10.41	

More recently, biogenic HAP of different origins, such as fish and cow bones, bone chars and food waste, has also been used. Accordingly, a low-crystalline form of a carbonated hydroxyapatite has been commercialised under the trade name of Apatite II^{TM}. The economically feasible use of Apatite II^{TM} to stabilise metal pollution in soils [20] and to remove Zn, Pb, Cd and U from groundwater is being developed [10,11,22].

Most of the literature on metal removal by HAP only provides information regarding batch experiments, which is interpreted as sorption isotherms [14,23–26]. Accordingly, metal removal processes have not been completely identified. Sugiyama et al. [27] suggested two general mechanisms for the ability of hydroxyapatite to take up divalent metal cations: (a) the first is concerned with the adsorption of ions on the solid surface face followed by their diffusion into hydroxyapatite and the release of cations originally contained within hydroxyapatite (ion–ion exchange mechanism) and (b) the second involves the dissolution of the hydroxyapatite in the aqueous solution containing divalent metals followed by the precipitation or co-precipitation of metal phosphates (dissolution–precipitation mechanism). However, Elouear et al. [25] and Valsami-Jones et al. [28] suggested that the dissolution–precipitation mechanism operates at a low pH (<4), whereas at a higher pH, the removal of metals is attributed to surface sorption or/and complexation. Thus, there have been few experimental studies conducted to identify the main chemical reactions and the mineral phases formed during the treatment steps.

Unlike batch experiments, flow-through columns allow the system to operate continuously and precipitate a sufficient mass of solid phases for identification. Moreover, these experiments supply information regarding the physical chemical aspects that affect the changes in the porosity and permeability of the reactive media. They are also very useful in determining the changes in the effluent composition due to the competition between the dissolution–precipitation rates and the water flux.

Apatite II^{TM} has proved suitable for reducing Zn and Pb to concentrations below regulatory levels in aquifers and infiltration ponds [29]. The present work investigates the removal capacity of Cd, Cu, Ni, Co and Hg by Apatite II^{TM} using column experiments to emulate large-scale passive remediation systems. This group of divalent metals is scarcely removed by using the standard technologies of AMD with calcite and calcite organic matter mixtures.

2. Experimental

2.1. Materials

The apatite used in this study was Apatite II^{TM} (US Patent #6,217,775), a biogenically precipitated material that is derived from fish bones with the general composition $Ca_{10-x}Na_x(PO_4)_{6-x}(CO_3)_x(OH)_2$, where $x < 1$. A total of 30–40 wt.% of organic materials is found in the internal porosity of the inorganic structure [11]. XRD patterns show that the raw material mainly consists of hydroxyapatite with a calcite content of *up to* 5 wt.%. The grain size of the samples ranged from 0.5 to 3 mm. The initial BET surface area was $1.9 \pm 0.2\ m^2\ g^{-1}$. The final BET surface area was measured in most of the experiments and ranged from 1 to $100\ m^2\ g^{-1}$ (Table 1).

2.2. Methods

Column experiments were designed to measure the reactivity of Apatite II^{TM} under flow conditions similar to those expected in transmissive aquifers. Solutions were administered continuously through Teflon tubing connected to a Gilson Minipuls® peristaltic pump. The inlet fluxes employed are shown in Table 1. Inflowing solutions were prepared either with a sulphate–metal salt or with a nitrate–metal salt and ultrapure Milli-Q water. With the exception of Hg, the sulphate concentration was controlled to be 10.41 mM ($1000\ mg\ L^{-1}$) by adding sodium sulphate (reagent grade, Merck) to simulated AMD waters. The pH of the inflowing solutions ranged from 2 to 5 (Table 1). The initial concentrations of Cd, Cu, Ni, Co and Hg ranged between 0.37 and 1.28 mM (Table 1). The pH was measured in sealed flow-through cells placed at the exit of the columns. Effluent solutions were filtered through a 0.45-μm filter and acidified with HNO_3 to pH < 1. The concentration of the cations was measured by inductively coupled plasma atomic

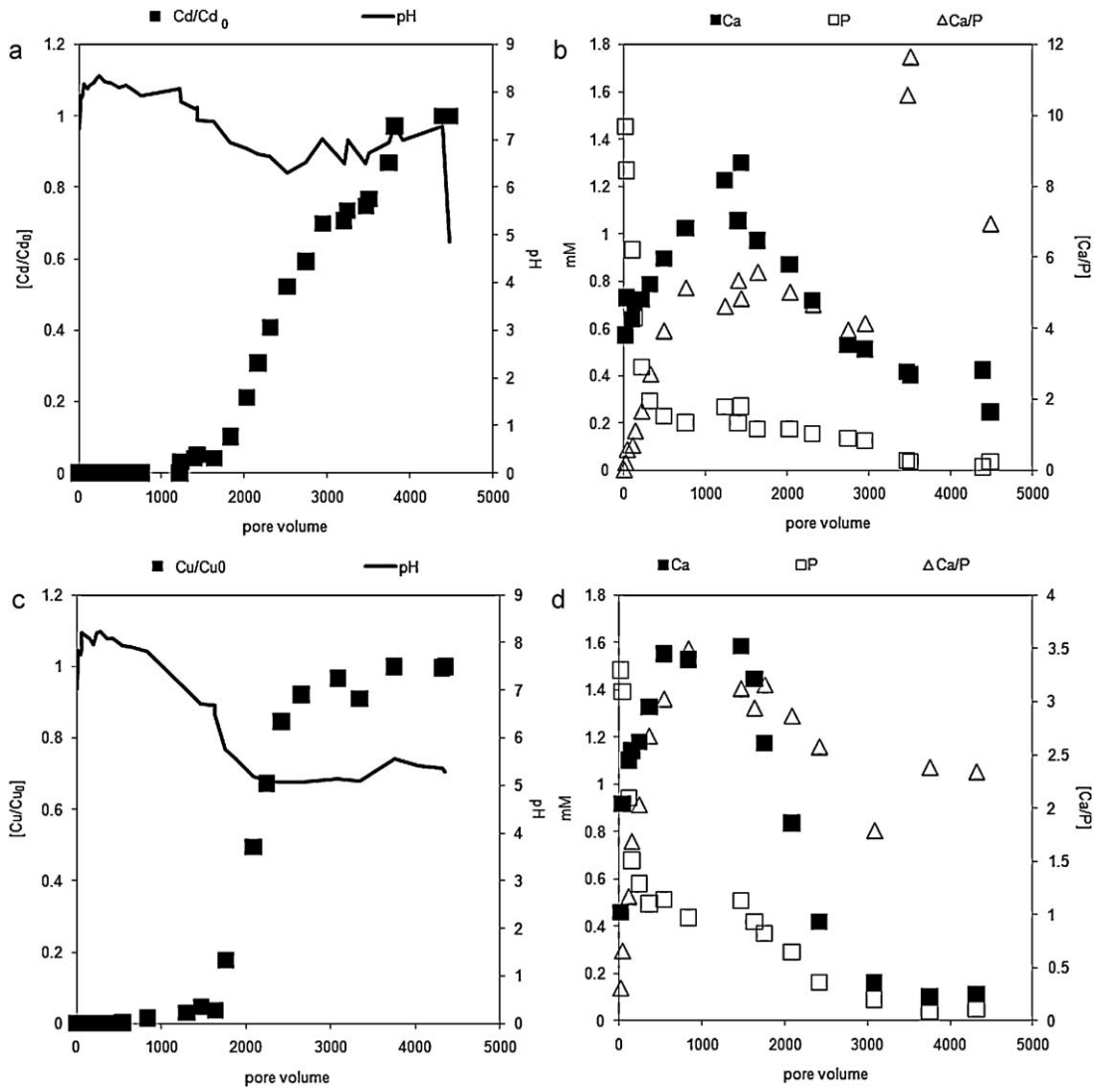

Fig. 1. Variation of (a) pH and [Cd]/[Cd_0] and (b) Ca, P and Ca/P molar ratio, as a function of pore volumes, of the outlet solution in the experiment with Cd. Evolution of (c) pH and [Cu]/[Cu_0] and (d) Ca, P and Ca/P, as a function of pore volumes of the outlet solution in the experiment with Cu (Cd_0 and Cu_0 are initial concentration of Cd and Cu in each experiment).

emission spectroscopy (ICP-AES). The accuracy of the measurements was approximately 3%. Flow rates were determined gravimetrically.

Tracer tests were conducted by adding a known concentration of acetone to the infiltrating solution to determine the effective porosity and hydraulic dispersivity. The outflowing solutions were introduced into a Hewlet-Packard HP53® spectrophotometer using a flow-through cuvette for the continuous monitoring of acetone. The measured pore volumes of the different columns are given in Table 1.

After the conclusion of the experiments, the reacted material of the columns was examined using a JEOL 3400® scanning electron microscope with an energy dispersive system (SEM–EDS). Crystal phases in the final column fillings were identified with a BRUKER D5005® X-Ray Diffractometer (XRD) with Cu Lα radiation.

3. Results and discussion

3.1. Cadmium and copper removal

Two solutions at pHs 4.9 and 4.8 and with 0.67 mM Cd and 1.18 mM Cu (75 mg L^{-1} of Cd and Cu, respectively), were used as input solutions (Table 1, experiments 1 and 2). The experiments lasted 13 and 10 months for Cd and Cu, respectively. The variation in the concentration of Cd, Cu, P and Ca and pH, as a function of pore volumes, is shown in Fig. 1a–d.

In both experiments, during the first 1000 pore volumes, the pH was maintained at approximately 8, and the Ca concentration increased as the P concentration sharply decreased (Fig. 1b and d). Then, the Ca concentration and pH decreased gradually as the P concentration remained more or less steady and then decreased gently. Phreeqc calculations show that the solution was undersaturated with respect to calcite in the first pore volumes of the experiment. The fast dissolution of calcite in the early stages raised the solution pH to 7–7.5 and increased the Ca concentrations. Thereafter, calcite was consumed, and the pH decreased to 6–7, suggesting Apatite II™ control.

Cd and Cu were removed from the solution to approximately 1500 pore volumes (Fig. 1a and c). The molar ratio of Ca/P output was higher than 1.67 (the stoichiometric Ca/P molar ratio of Apatite II™) in both cases due to aqueous phosphorus deficiency. This result is attributed to P removal because of the precipitation of cadmium and copper phosphates.

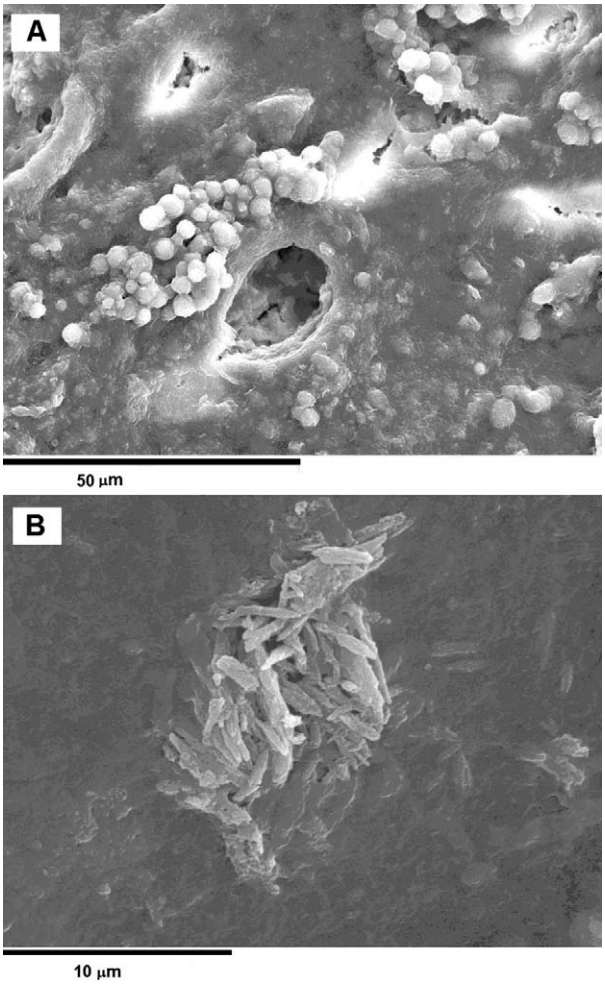

Fig. 2. SEM images: (A) amorphous layers of precipitates of Cd–P–O covering the Apatite II^{TM} grains and also spherical aggregates on top of the Apatite II^{TM} surface; (B) small crystals with a needle-like habit in the surface of the amorphous layer.

XRD patterns of newly precipitated material revealed the absence of detectable crystalline phases in the Cd column. The SEM–EDS examination detected the presence of layers of precipitates of Cd–P–O without crystalline forms covering the Apatite II^{TM} grains. Spherical aggregates or small elongated crystals were also found on the surface of the Cd–P–O layer (Fig. 2a and b).

The solubility data of $Cd_3(PO_4)_2(s)$, $Cd_5H_2(PO_4)_4(s)$ and $Cd_5(PO_4)_3OH(s)$ mineral phases were used to evaluate the variation in the Cd concentration with pH during the column experiment (Fig. 3a). The concentration of aqueous Cd, P and H^+ in the outlet solution was in accordance with that expected for equilibrium with cadmium phosphate $Cd_3(PO_4)_2(s)$; this resulted in the fact that the removal of Cd could be associated with the formation of this solid phase. The evolution of the corrected molar ratio Ca/P ($[Ca]^*/[P]^*$) after taking into account the stoichiometric amount of P consumed during the precipitation of $Cd_3(PO_4)_2(s)$, $Cd_5H_2(PO_4)_4(s)$, and $Cd_5(PO_4)_3OH(s)$ along the experiment lifetime is given in Table 2.

The $[Ca]^*/[P]^*$ molar ratio was calculated from the total Ca and P concentrations ($[Ca]_{measured}$ and $[P]_{measured}$), taking into account the amount of P consumed ($[P]_{consumed}$) during the precipitation of the postulated metal phosphate phases ($M_r(PO_4)_q$).

$$[Ca]_i^* = [Ca]_{measured(i)}$$

$$[P]_i^* = [P]_{measured(i)} + [P]_{consumed(i)}$$

$$= [P]_{measured(i)} + ([[M]_o - [M]_i) * \left(\frac{q}{r}\right)$$

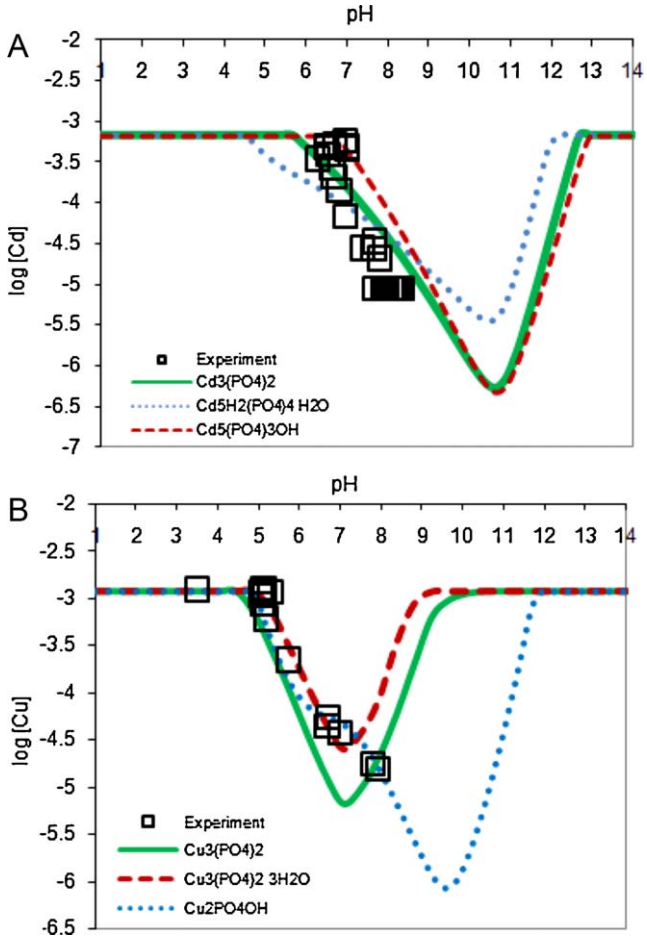

Fig. 3. Variation of measured Cd(II) (A) and Cu(II) (B) concentrations with pH and metal concentration in equilibrium with other Cd and Cu phases using the MINTEQ database [50].

where $[M]_o$ and $[M]_i$ are the total inlet and outlet metal concentrations and q and r are the stoichiometric coefficients of the metal phosphate ($M_r(PO_4)_q(s)$), respectively. As can be seen, the formation of $Cd_3(PO_4)_2(s)$ gives Ca/P ratios that approach the expected value of 1.67 (the stoichiometric molar ratio Ca/P for Apatite II^{TM}).

In the literature, the retention mechanism of Cd has commonly been interpreted by surface complexation and ion-exchange mechanisms [20,30–32]. However, the dissolution of HAP and the formation of a new stable phase of Cd–apatite on the surface of HAP particles of cadmium phosphate have been interpreted from batch experiments. Jeanjean et al. [33] and later Mandjiny [34] concluded that Cd reacted with Apatite II^{TM} by initial sorption followed by slower intercrystalline diffusion and cation exchange with Ca ions. Thus, Cd is ultimately incorporated into the bulk of the host Apatite II^{TM} as a $Cd_5H_2(PO_4)_5(s)$ phase [33]. Similarly, Valsami-Jones et al. [28] reported that the removal of Cd by synthetic hydroxyapatite was pH-dependent and proposed that Cd forms a mixed cadmium–calcium phosphate ($Cd_xCa_{5-x}(PO_4)_3OH(s)$). In contrast, our results suggest that the removal of Cd by the formation of $Cd_3(PO_4)_2(s)$ provides a better description of the column breakthrough data.

For copper column experiments, the XRD patterns of newly precipitated material revealed no crystalline phases. The SEM–EDS examination of the precipitates showed the presence of an amorphous precipitate layer on the surface of Apatite II^{TM} grains with the presence of Cu–P–O (Fig. 4).

The solubility data of $Cu_3(PO_4)_2(s)$, $Cu_3(PO_4)_2 3H_2O(s)$ and $Cu_2(PO_4)OH(s)$ were used to evaluate the variation of the measured

Table 2
Ca^*/P^* molar ratio[a] evolution along column breakthrough experiments for Cd, Cu, Ni, Co and Hg assuming the formation of the metal–phosphates.

Cd												
Pore volume	36	170	215	245	323	382	486	572	756	1221	1233	1397
$Cd_5H_2(PO_4)_4\ H_2O$	0.40	0.66	0.74	0.84	0.95	0.98	1.06	1.16	1.24	1.36	1.47	1.33
$Cd_3(PO_4)_2$	0.43	0.72	0.82	0.93	1.07	1.11	1.20	1.32	1.42	1.54	1.66	1.52
$Cd_5(PO_4)_3OH$	0.44	0.76	0.86	0.99	1.14	1.19	1.29	1.42	1.53	1.65	1.78	1.63
Cu												
Pore volume	40	242	276	363	429	543	638	838	1302	1473	1635	1637
$Cu_2(PO_4)OH$	0.46	1.01	1.11	1.22	1.33	1.41	1.43	1.50	1.46	1.47	1.49	1.35
$Cu_3(PO_4)_2$	0.42	0.86	0.95	1.04	1.13	1.20	1.21	1.26	1.23	1.25	1.27	1.14
Ni												
Pore volume	41	118	156	198	250	285	375	443	561	610	660	872
$Ni_3(PO_4)_2$	0.55	0.68	0.76	0.85	0.96	1.09	1.29	1.44	1.32	1.33	1.40	1.46
Co												
Pore volume	30	73	276	314	410	484	611	716	938	1502	1517	1735
$Co_3(PO_4)_2 8H_2O(s)$	0.35	0.59	1.00	1.10	1.21	1.18	1.25	1.27	1.27	1.21	1.56	1.68
Hg												
Pore volume	12	78	90	130	203	264	390	566	695	719	833	849
$HgHPO_4$	1.26	1.55	1.74	1.64	1.63	1.69	1.71	1.92	2.04	1.09	2.33	2.37
$Hg_3(PO_4)_2$	1.33	1.66	1.83	1.73	1.71	1.78	1.79	1.95	2.06	1.10	2.17	2.23

[a] The $[Ca]^*/[P]^*$ molar ratio has been calculated from the total Ca and P measured concentrations ($[Ca]_{measured}$ and $[P]_{measured}$) and taking into account the amount of P consumed for the precipitation ($[P]_{consumed}$) of the postulated metal phosphate phases ($M_r(PO_4)_q$) $[Ca]_i^* = [Ca]_{measured(i)}$. $[P]_i^* = [P]_{measured(i)} + [P]_{consumed(i)} = [P]_{measured(i)} + ([M]_o - [M]_i)^*(q/r)$ where $[M]_o$ and $[M]_i$ are the total inlet and outlet metal concentrations and q and r are the stoichiometric coefficients of the metal phosphate with formulae ($M_r(PO_4)_q$).

concentration of Cu(II) with pH (Fig. 3b). Aqueous Cu, P and H^+ concentrations in the outlet solution were in accordance with those expected from equilibrium with the copper-hydroxyl-phosphate $Cu_2(PO_4)OH(s)$. The evolution of the corrected molar ratio Ca/P ($[Ca]^*/[P]^*$), assuming the precipitation of $Cu_3(PO_4)_2(s)$,and $Cu_2(PO_4)OH(s)$, along the experiment lifetime is given in Table 2. The formation of $Cu_2(PO_4)OH(s)$ results in Ca/P ratios that approach the expected value of 1.67.

A large number of batch experiments [14,19,23,35–37] suggest sorption processes as the removal mechanism of copper by hydroxyapatite. However, the dissolution of HAP and precipitation of amorphous copper phosphates ($Cu_3(PO_4)_2(s)$) and libethenite ($Cu_2(PO_4)OH(s)$) have also been described in experiments with phosphate rocks, synthetic HAP and fish bones [27,38,39]. Our results fully agree with the formation of $Cu_2(PO_4)OH(s)$ as proposed by the latter group of authors.

3.2. Nickel and cobalt removal

The solutions used to study the remediation of Ni and Co contained 1.28 and 1.27 mM (75 mg L^{-1}) of Ni and Co, respectively (Table 1, experiments 3 and 4). The experiments lasted 10 months for Ni and 16 for Co. The evolution of the concentrations of P, Ca, Ni and Co and pH as a function of pore volume is shown in Fig. 5.

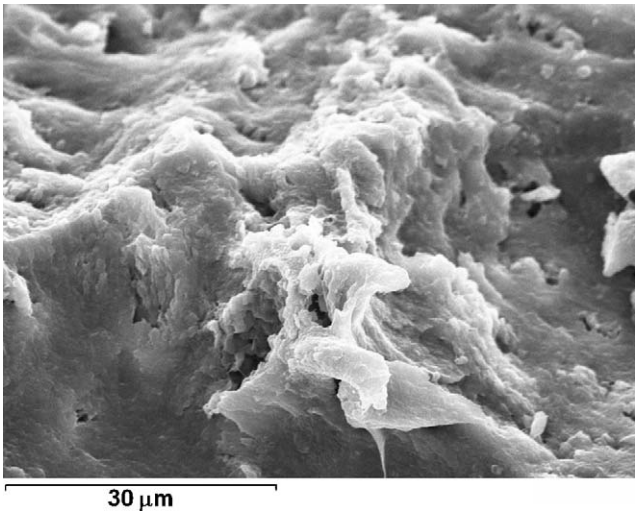

Fig. 4. SEM image of amorphous precipitate layer on the surface of Apatite II™ grains with presence of Cu–P–O.

Just as in the experiments used to study Cd and Cu, calcite dissolution caused the pH to increase up to 7.5–8. After the consumption of calcite, the pH dropped to 6.5–7.5 in both experiments, which suggests control by Apatite II™ (Fig. 5a and c). At this stage, both Ni and Co were removed from the solution, which resulted in concentrations below 0.00015 mM. During this period, the Ca/P molar ratio was higher than 1.7. This phosphorus deficiency in the solution was caused by the precipitation of the metal phosphate.

For Ni, the removal was completed, and the Ca/P ratio returned to the stoichiometric molar ratio of Apatite II™ after 1500 pore volumes. Then, the drop in pH was associated with the passivation of the Apatite II™ reactive surface because of the formation of nickel precipitates. The pH of the outflow was kept constant at approximately 7, whereas the Ni concentration reached the input value of 1.28 mM (75 mg L^{-1}) (Fig. 4a).

In the case of Co, passivation was not observed, and the remedial capacity continued for almost 7000 pore volumes. As a result, 70–80% of Co of the solution was retained by Apatite II™ (Fig. 5c). After 3000 pore volumes, the retention capacity diminished, and the C/C_o approached 1, whereas the pH was maintained at approximately 6.5. When the pH rose again to values between 7 and 7.5, the C/C_o ratio decreased again to values below 0.8. The trend in the evolution of Ca and P concentrations showed that the Ca/P molar ratio was higher than 1.7 along the experiment lifetime because of an aqueous phosphorus deficiency. This effect is attributed to P removal because of the precipitation of cobalt phosphate.

The XRD patterns of newly precipitated material in the two columns revealed an absence of crystalline phases. The SEM–EDS examination of the sample from the Ni column confirmed the presence of an amorphous Ni–P–O layer on the surface of the particles. Moreover, the aqueous Ni concentration was in accordance with that expected from a solution equilibrated with $Ni_3(PO_4)_2$ as shown in Fig. 6a. The evolution of the corrected molar ratio Ca/P, assuming the precipitation of $Ni_3(PO_4)_2(s)$, along the experiment lifetime is given in Table 2. As can be seen, the formation of $Ni_3(PO_4)_2(s)$ provides corrected Ca/P ratios ($[Ca]^*/[P]^*$) that approach the expected value of 1.67.

There are few studies on Ni(II) removal with phosphates reported in the literature. Bostick [40] observed a low affinity of Ni(II) to sorb onto Apatite II. Using synthetic hydroxyapatite

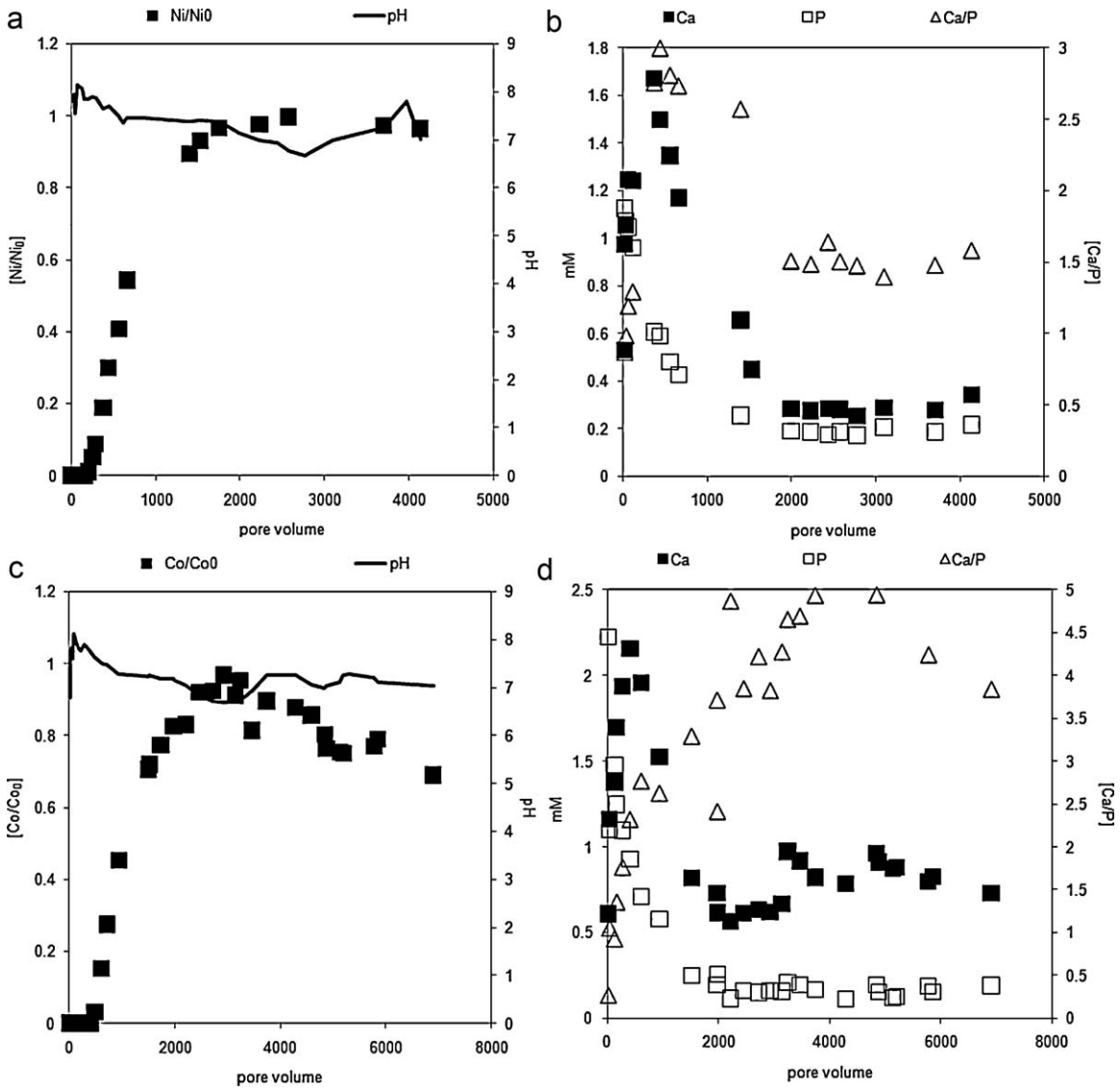

Fig. 5. Variation of (a) pH and [Ni]/[Ni_0] and (b) Ca, P and Ca/P molar ratio, as a function of pore volumes, of the outlet solution in the experiment with Ni. Evolution of (c) pH and [Co]/[Co_0] and (d) Ca, P and Ca/P, as a function of pore volumes of the outlet solution in the experiment with Co (Ni_0 and Co_0 are initial concentration of Ni and Co in each experiment).

columns, Suzuki et al. [16] found that an appreciable amount of Ni(II) could be removed assuming a cation-exchange mechanism, and ranked the exchange affinity as Cd(II), Zn(II) > Ni(II) > Ba(II), Mg(II). The removal of Ni by phosphate amendments was also investigated by Perrone et al. [41], Elouear et al. [42] and Mobasherpour et al. [43] and results strongly support the ion exchange as the main mechanism for Ni^{2+} removal. Nickel uptake involves rapid surface complexation of the Ni^{2+} ions on the ≡POH sites before the formation of a compound of formula $Ca_{10-x}Ni_x(PO4)_6(OH)_2$. However, Sowder et al. [44], using hydroxyapatite for reducing nickel availability in sediments, suggested that nickel forms $Ni_3(PO_4)_2{\cdot}7H_2O$. Moreover, because of the existence of mixed nickel–calcium phosphate minerals (e.g., cassidyite and hydrated calcium nickel magnesium phosphate), these authors suggested that synergistic co-precipitation may occur. Our findings agree with those of Sowder et al. [44]. Moreover, the removal of Ni is much lower than that of Cd and Zn and is in agreement with the exchange rank reported by Suzuki et al. [16].

For the Co column, XRD patterns of the reacted material revealed the presence of $Co_3(PO_4)_2 8H_2O$(s). SEM–EDS examination also confirmed the presence of a non-crystallised Co–P–O layer on the

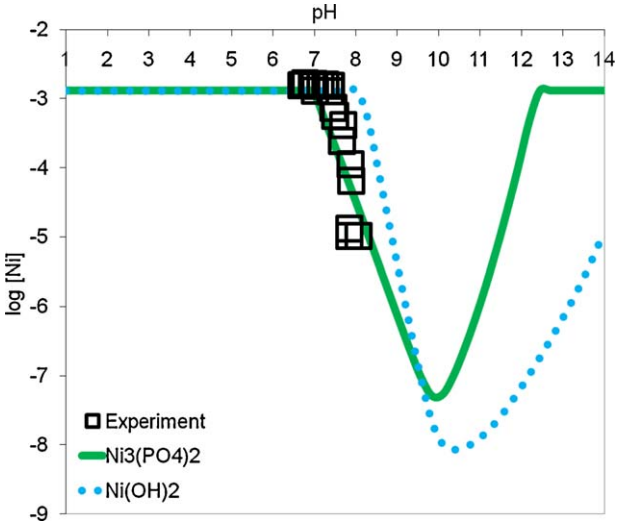

Fig. 6. Variation of Ni(II) concentration with pH of the outlet solutions. Plotted metal concentrations in equilibrium with the phosphorus solid phases were calculated using the speciation code HYDRA [50].

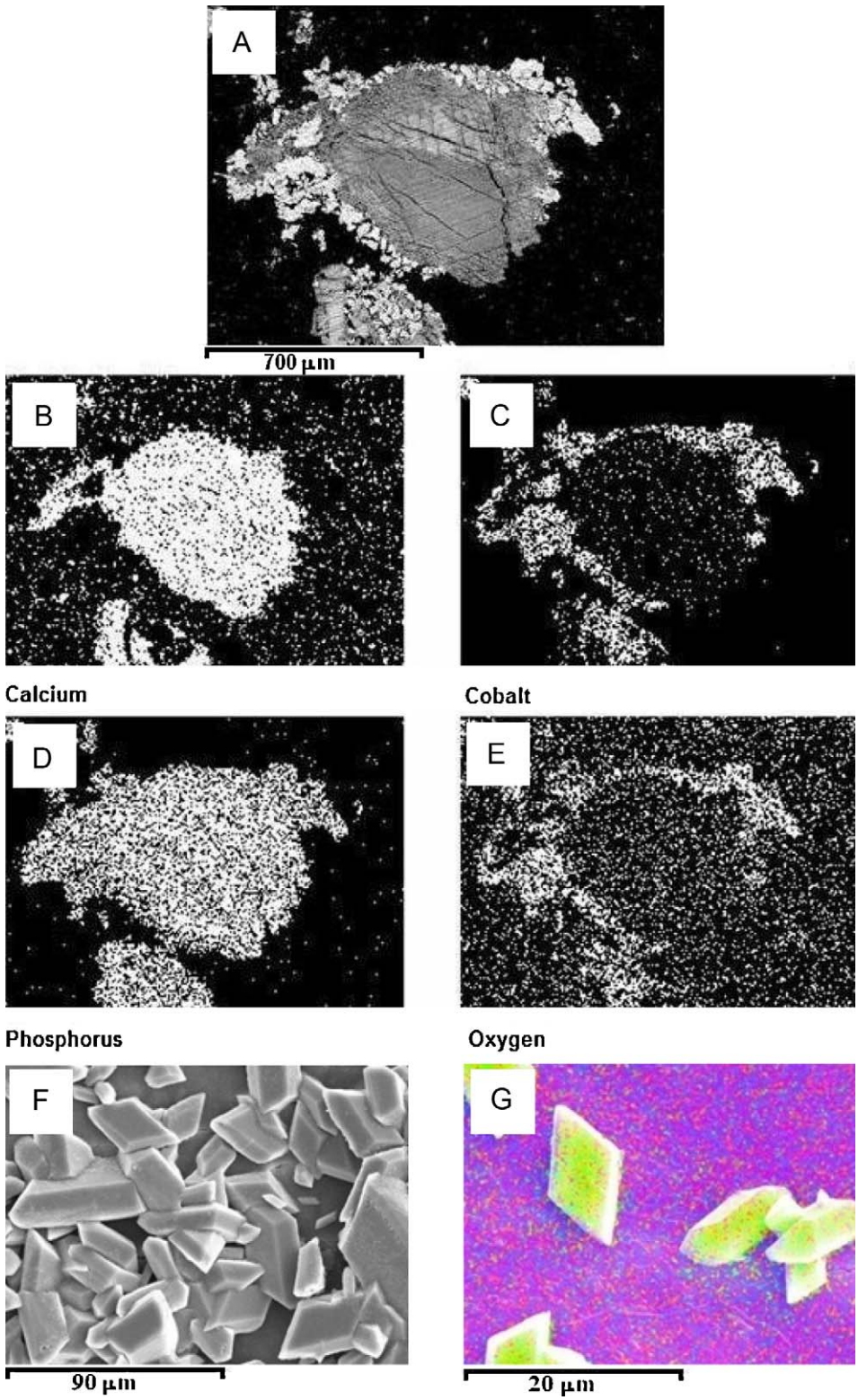

Fig. 7. SEM images: (A) section of precipitate of cobalt; (B)–(E) Element mapping. Yellow represents cobalt. Blue calcium and red phosphorus. The rhombic crystals on the surface of the particles (F). Element mapping showing the rhombic crystals distribution on the sample (G), the yellow colour is cobalt, the blue colour is calcium and the red colour is phosphorus. (For interpretation of the references to colour in this figure legend, the reader is referred to the web version of the article.)

surface of the particles. Rhombic crystals containing mainly Co–O were also observed on top of this layer (Fig. 7a and f). Moreover, the mapping of the particle shows that the Co–P–O-rich layer is located around the particle, whereas the inner region is rich in Ca–P–O (Fig. 7b–e). In addition, the oxygen content of the precipitates is higher and the phosphorous content lower than that of the Apatite II^{TM} core, suggesting the presence of cobalt oxides or hydroxides (Fig. 7g).

The aqueous Co concentration was in accordance with that expected from the equilibrium with $Co_3(PO_4)_2 8H_2O(s)$ (Fig. 8).

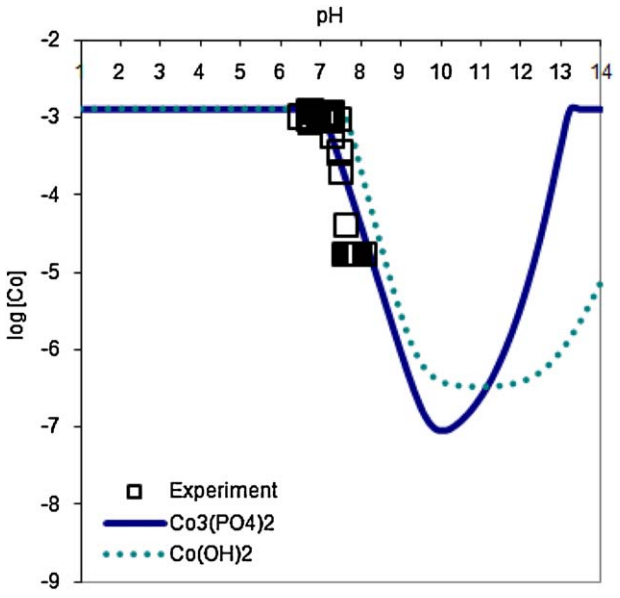

Fig. 8. Variation of measured Co(II) concentrations with pH and metal concentration in equilibrium with other Co phases using the MINTEQ database [50].

The formation of $Co(OH)_2$ could occur at the end of the breakthrough point, at which Apatite II^{TM} is exhausted and the amount of phosphate decreases. This effect could account for the last part of the breakthrough curve after 3000 pore volumes, in which the C/C_o reaches values close to 0.8 and the formation of $Co(OH)_2(s)$ is favoured in the absence of dissolved phosphate. The proposed removal mechanism could be a mixed process of precipitation in which cobalt phosphate is initially precipitated followed by hydroxide when the hydroxyapatite source is exhausted.

The evolution of the corrected molar ratio Ca/P ($[Ca]^*/[P]^*$), assuming the precipitation of $Co_3(PO_4)_2 8H_2O(s)$ and $Co(OH)_2(s)$, along the experiment lifetime is given in Table 2. The formation of $Co_3(PO_4)_2 8H_2O(s)$ results in Ca/P ratios that approach the expected value of 1.67.

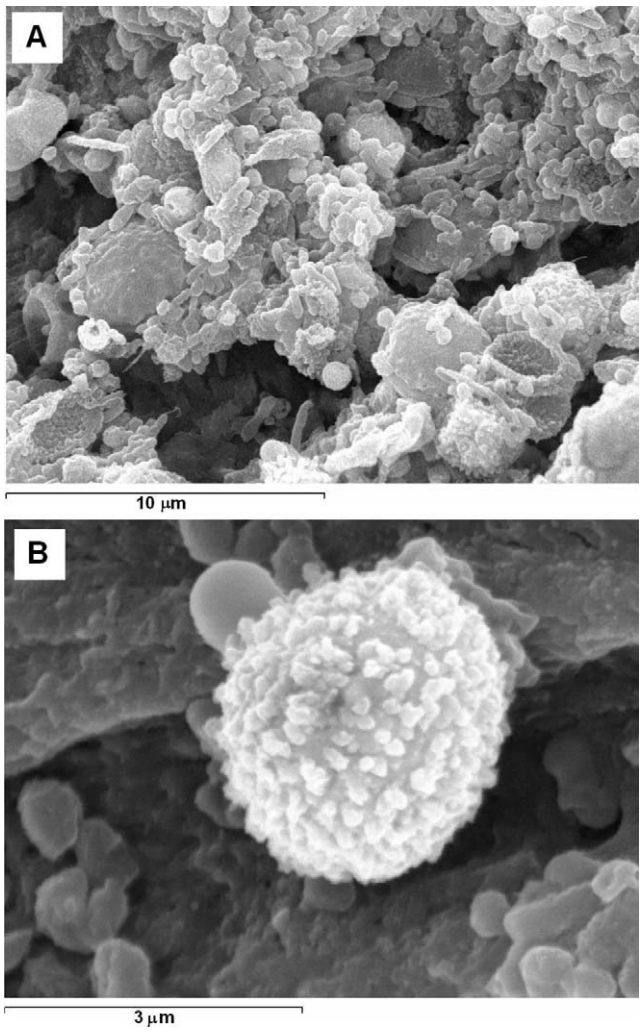

Fig. 10. SEM image: (A) amorphous spherical-like particles of Hg–P–O on the surface the Apatite II^{TM} grains; (B) crystalline phases on the surface of precipitated amorphous ball on the surface of Apatite II^{TM}.

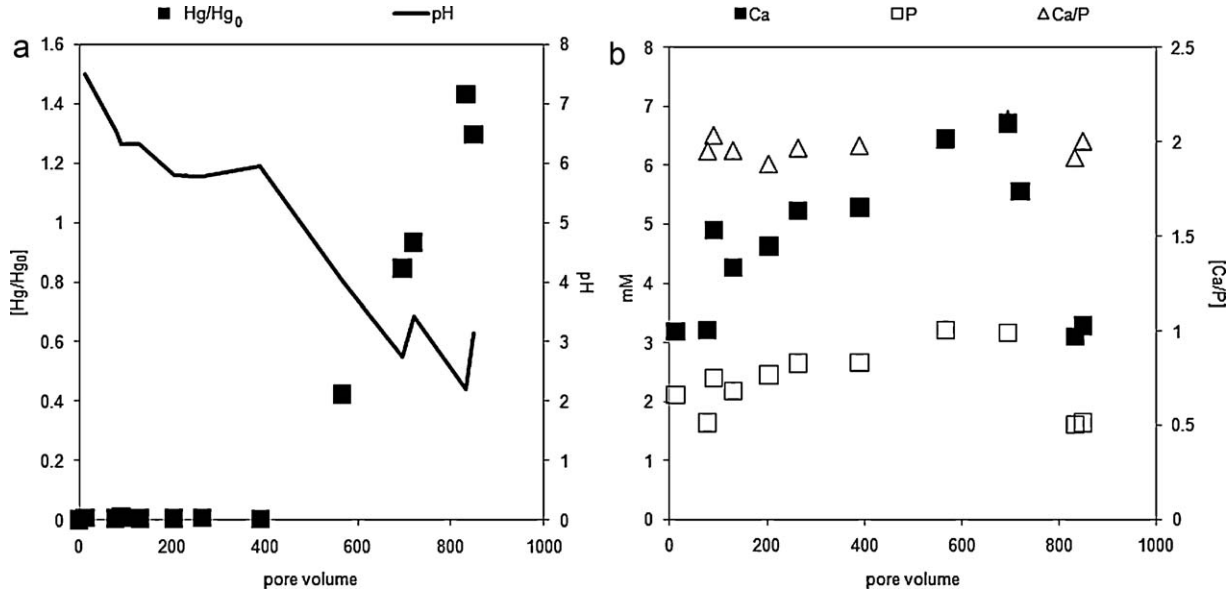

Fig. 9. Variation of (a) pH and [Hg]/[Hg_0] and (b) Ca, P and Ca/P molar ratio, as a function of pore volumes, of the outlet solution in the experiment with (Hg_0 is the initial concentration of Hg in the experiment).

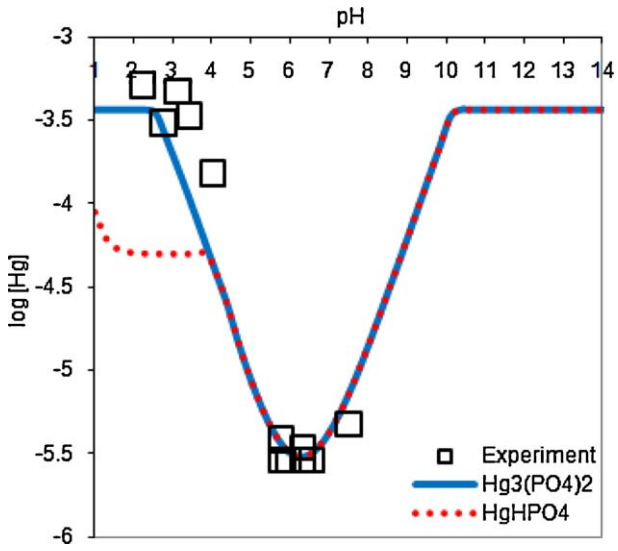

Fig. 11. Variation of measured Hg(II) concentrations with pH and metal concentration in equilibrium with other Hg phases using the MINTEQ database [50].

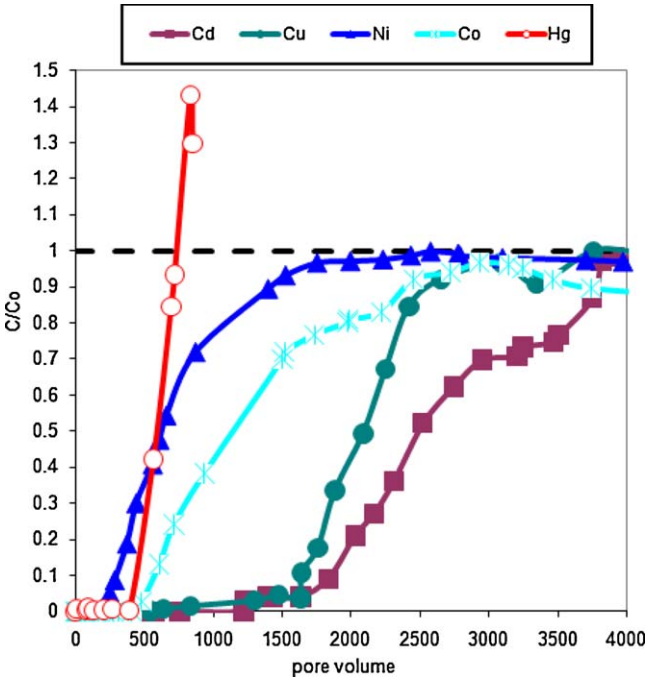

Fig. 12. Variation of concentration ratio of the outlet solution in each experiment as a function of pore volumes.

In the literature, cobalt removal using hydroxyapatites has been described by sorption and ion-exchange processes. Studying the use of synthetic hydroxyapatite, Gómez del Río et al. [45] concluded that the removal of Co, Zn and Cd could be modelled by a mechanism of non-ideal ion exchange with the affinities ranked as Cd > Zn ≈ Co. Based on experiments using animal bones, Dimovic et al. [46] and Pan et al. [47] also proposed ion exchange with Ca^{2+} and specific cation sorption as the main removal mechanisms. The amount of Co^{2+} desorbed from loaded bone sorbents increased with the decrease in pH and with the increase in Ca^{2+} concentration when pH > 8, at which the precipitation of cobalt hydroxide occurred. Similarly, using synthetic $Ca_{10}(PO_4)_6(OH)_2$(s), Smiciklas et al. [48] showed results that strongly supported ion exchange as the main mechanism for Co^{2+} removal. Only Sugiyama et al. [27], who used different calcium phosphate sources, suggested that calcium hydrogen phosphate removed Co^{2+} as amorphous phosphate phases. Our findings are similar to these results.

3.3. Mercury removal

A solution containing 0.37 mM (75 mg L^{-1}) of Hg at pH 2 was used as input (Table 1, experiment 5). Mercury nitrate was used in this case to prevent the precipitation of mercury sulphates. The experiment lasted for only four months because the high acidity of the input solution rapidly dissolved Apatite II^{TM}. The evolution of P, Ca and Hg concentrations and pH as a function of pore volume is shown in Fig. 9.

As in the other experiments, the pH reached values of 7–7.5. After the consumption of calcite, the pH fell to 6–7, suggesting control by II^{TM}. At this stage, Hg was recovered from the solution, yielding concentrations below 0.005 mM. During this period, the Ca/P molar ratio was slightly higher than 1.7, owing to the depletion of dissolved phosphorus, which was consumed by the precipitation of mercury phosphate. After 400 pore volumes, the pH value fell to 2–3, i.e., the initial pH value, along with a drop in the concentration of Ca and P (Fig. 9b). Mass balance calculations show that more than 60 wt.% of the initial Apatite II^{TM} was consumed.

As was observed for the other metals, the pH drop is associated with a reduction in the Apatite II^{TM} reactive surface area caused by the formation of mercury phosphate. When the pH fell below 3, the concentration of mercury reached 1.4 mM (107 mg L^{-1}), far above the input value of 0.37 mM (Fig. 9a). This excess is attributed to the dissolution of the previously precipitated Hg phosphate.

No crystalline phases were detected in the analysis of XRD patterns of the materials recovered. SEM–EDS examination confirmed the presence of a Hg–P–O layer on the surface of HAP grains (Fig. 10a) and the formation of spherical-like aggregates top (Fig. 10b).

The solubility data for the $Hg_3(PO_4)_2$(s) and $HgHPO_4$(s) phases were compared with the experimental pH and Hg concentrations

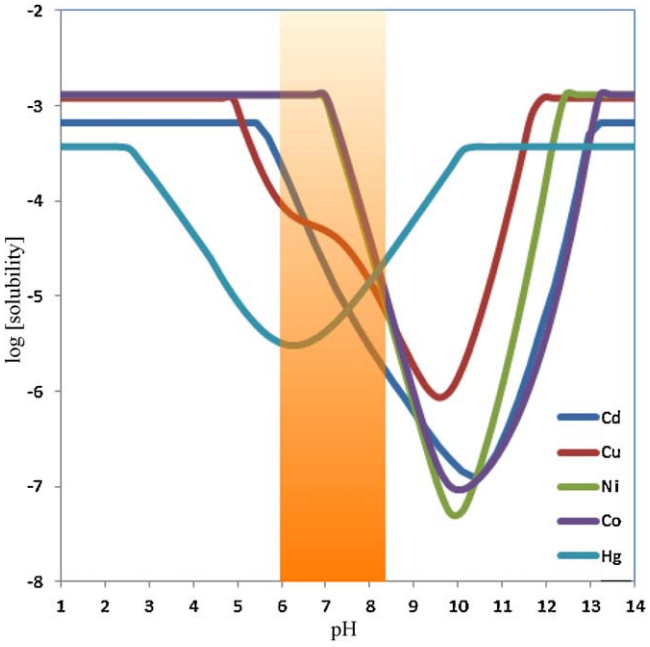

Fig. 13. Variation of metal concentrations in equilibrium with the metal phosphates using the speciation code HYDRA and MINTEQ database [50]. The shaded rectangular field indicates the pH range yielded using hydroxyapatite as a passive treatment of acid water.

Table 3
Retention capacities of different hydroxyapatites.

Metal	Hydroxyapatite resource	pH initial	pH final	S^a [mg/g]	S^b [mg/g]	Reference
Cadmium	Apatite II™	4.9	7.0	108	–	Column experiment (1)[c]
	Apatite II™	4.9	4.9	189	–	Column experiment (1)[d]
	Apatite II™	–	–	3.8	4.50	[40]
	Apatite II™	–	–	50	–	[21]
	Mineral	1–12	>6.2	73	–	[13]
	Mineral	2.0–6.0	–	–	10.46	[25]
	Synthetic	7.0	4.9	189	290	[18]
	Synthetic	–	7.9	–	32.00	[31]
	Synthetic	6.0	–	87.7	–	[51]
	Synthetic	5.0–7.0	4.0–4.5	16.7	–	[52]
	Synthetic	5.6	5.4	119.2	–	[53]
	Synthetic	3.0–12.0	–	41.7	67.6	[26]
	Synthetic	5.88–6.61	5.64–7.22	67	66.6	[54]
	Synthetic	5.0–8.0	6.0	–	260.42	[55]
	Nano hydroxyapatite synthetic	5.5	–	64.1	157.9	[56]
	Bone char	4.8	5.0	~63	58.5	[36]
	Activated mineral	2.6–6.0	–	–	13.56	[25]
	Carbonate hydroxyapatite synthesized	2.0–9.0	6.0	–	111.1	[57]
	Areca waste (food waste)	2.0–8.0	5.6	–	1.12	[37]
Copper	Apatite II™	4.8	6.5	76	–	Column experiment (2)[c]
	Apatite II™	4.8	5.1	99	–	Column experiment (2)[d]
	Apatite II™	5.9	6.6	6.8	4.80	[40]
	Apatite II™	–	–	50	–	[21]
	Mineral	5.5	–	–	8	[14]
	Mineral	2.0–6.0	–	–	9.8	[25]
	Synthetic	6.6	5.3	90.7	95.95	[23]
	Synthetic	5.0	4.4	52.5	57.3	[24]
	Synthetic	5.5	5.5	26.7	–	[58]
	Bone char	4.8	5.0	~50	45.8	[36]
	Activated mineral	2.6–6.0	–	–	13.28	[25]
	Carbonate hydroxyapatite synthesized	2.0–9.0	6.0	–	142.9	[57]
	Areca waste (food waste)	2.0–8.0	5.6	–	2.84	[37]
Nickel	Apatite II™	5.0	7.9	12	–	Column experiment (3)[c]
	Apatite II™	5.0	7.4	37	–	Column experiment (3)[d]
	Apatite II™	7.3	6.7	7.4	7.9	[40]
	Apatite II™	–	–	50	–	[21]
	Mineral	2.0–11.0	–	–	7.63	[42]
	Nano hydroxyapatite synthetic	6.6	–	48.75	46.17	[43]
Cobalt	Apatite II™	5.0	7.5	24	–	Column experiment (4)[c]
	Apatite II™	5.0	6.7	160	–	Column experiment (4)[d]
	Apatite II™	–	–	50	–	[21]
	Synthetic	4.0–8.0	5.1	20.19	20.92	[48]
	Swine bone char	2.0–9.0	–	18.37	108.7	[47]
	Animal bones	5.0	–	28.9	29.2	[46]
Mercury	Apatite II™	2.0	5.9	38	–	Column experiment (5)[c]
	Apatite II™	2.0	3.4	54	–	Column experiment (5)[d]
	Apatite II™	3.1	6.8	0.79	0.67	[40]
	Apatite II™	–	–	50	–	[21]

[a] Is the capacity of retention, in mg of metal for g of retention material.
[b] Is the maximum sorption capacity by isotherm, in mg of metal for g of retention material.
[c] Is the capacity of retention in time of break in the experiment.
[d] Is the top value in the experiment.

(Fig. 11). The concentration of aqueous Hg, P and H^+ in the outlet solution was in accordance with equilibrium with $Hg_3(PO_4)_2(s)$. Therefore, the removal of Hg could be associated with the formation of this solid phase.

The evolution of the corrected molar ratio Ca/P ($[Ca]^*/[P]^*$), assuming the precipitation of $Hg_3(PO_4)_2(s)$ and $HgHPO_4(s)$, along the experiment lifetime is shown in Table 2. As can be seen, the formation of $Hg_3(PO_4)_2(s)$ provides Ca/P ratios that approach the expected value of 1.67.

There are only a few studies of the removal of Hg(II) with hydroxyapatites in the literature. Narasaraju and Phebe describe the substitution of Ca(II) by several divalent metal cations in the II™ structure [49]. More recently, after evaluating the capability of Apatite II to remove metals, Bostick [40], found a strong affinity of Hg to sorb onto the surface of the mineral. In contrast, the results of the present study suggest the removal of mercury by the formation of $Hg_3(PO_4)_2(s)$.

3.4. Loadings capacity

The breakthrough curves obtained for different metals are compared in Fig. 12. We assume that the metal was no longer removed when its concentration in the output was 10% of the inflow concentration ($C/C_o = 0.1$). This break point was reached after 1800 pore volumes for Cd and 1600 for Cu. These values correspond to a retention capacity of 92 mg Cd/g Apatite II™ (48 mg/m^2) and 65 mg Cu/g Apatite II™ (34 mg/m^2). In the Ni and Co columns, the exhaustion of Apatite II™ occurred before the break point was reached at 300 and 600 pore volumes for Ni and Co, respectively. These results correspond to a retention of 23 mg Ni/g Apatite II™ (12 mg/m^2) and 11 mg Co/g Apatite II™ (6 mg/m^2).

The column was considered unreactive when the outflow metal concentration was similar to the inflow value ($C/C_o = 1$), which occurred after 4300, 3700, 2600 and 6900 pore volumes for Cd, Cu, Ni and Co, respectively The mass balance calculation shows that

only between 17 and 22 wt.% of the initial Apatite II^{TM} was consumed in the four experiments. Therefore, the decrease in pH to the input value and the passivation of the column were attributed to the coating of the Apatite II^{TM} surface and/or to the development of preferential flow paths caused by the precipitates (Fig. 13).

Unlike that of mercury, the pH of the input was as low as 2, and most of the Apatite II^{TM} was employed in neutralising acidity. The break point ($C/C_o = 0.1$) was attained after 500 pore volumes, yielding a retention capacity of 38 mg Hg/g Apatite II^{TM} (20 mg/m^2). The column was considered to be exhausted after 700 pore volumes and when 61% of the initial mass of Apatite II^{TM} was consumed.

Table 3 shows the retention of cadmium, copper, nickel, cobalt and mercury per gram of Apatite II^{TM} compared with retention rates using hydroxyapatites of non-biogenic origin and synthetic calcium phosphates.

4. Conclusions

The efficiency of Apatite II^{TM} increases as the acidity decreases. Therefore, the application of apatite-based materials for metal removal treatments should be restricted to slightly acid to neutral waters. This phenomenon is evident in the Hg column experiment, in which an inflow solution with pH 2 leads to a high consumption of Apatite II^{TM} Because of the preferred process of using phosphate ions to form metal–phosphate precipitates, the mixture with other sources of alkalinity, such as limestone, is proposed to extend the duration of Apatite II^{TM} (Fig. 13).

No clogging of the columns was observed. Compared with other reactive materials such as limestone and caustic magnesia that exhibit a reduction of porosity [29], Apatite II^{TM} showed stable hydraulic performance. The flow of 0.02 mL/min used in the experiments was equivalent to a Darcian velocity of 60 m^3/m^2/y. The capacity of Apatite II^{TM} to retain cadmium, copper, nickel, cobalt and mercury in transmissive aquifers should therefore be noted.

The extrapolation of the column durabilities to a 1-m-thick passive treatment suggests that the Apatite II^{TM} filling can be active between 5 and 10 years for an inflow pH exceeding 5. The mixture with limestone should be tested for more acidic waters.

Acknowledgements

We are grateful to J. Wright and J.L. Conca (PIMMS, UFA Ventures (USA)) for supplying the Apatite II^{TM} sample. We thank M. Marsal (UPC) for her helpful comments and SEM assistance and M. Cabañas and J. Elvira (CSIC) for the ICP-AES assistance. This work was funded by the Spanish Government projects CTQ2008-06842-C02-01/PPQ, CTM-2007-66724-CO2/TECNO, CGL2010-21956-CO2-01 and the Catalan Government project 2009SGR905.

References

[1] D.B. Johnson, K.B. Hallberg, Acid mine drainage remediation options: a review, Sci. Total Environ. 338 (2005) 3–14.
[2] A. Akcil, S. Koldas, Acid mine drainage (AMD): causes, treatment and case studies, J. Clean. Prod. 14 (2006) 1139–1145.
[3] Official Journal of the European Community. Directive 98/78/EC, 1998, control: 0378-6978, 40.
[4] USEPA, National Primary Drinking Water Standards; EPA 816-F-01-007, 2001, http://www.epa.gov/safewater.
[5] R. Thiruvenkatachari, S. Vigneswaran, R. Naidu, Permeable reactive barrier for groundwater remediation, J. Ind. Eng. Chem. 14 (2008) 146–156.
[6] D.W. Blowes, C.J. Ptacek, J.L. Jambor, In-situ remediation of Cr(IV)-contaminated groundwater using permeable reactive walls: laboratory studies, Environ. Sci. Technol. 31 (1997) 3348–3357.
[7] O. Gibert, J. de Pablo, J.L. Cortina, C. Ayora, Municipal compost-based mixture for acid mine drainage bioremediation: metal retention mechanisms, Appl. Geochem. 20 (2005) 1648–1657.
[8] T.S. Rötting, M.A. Caraballo, J.A. Serrano, C. Ayora, J. Carrera, Field application of calcite Dispersed Alkaline Substrate (calcite-DAS) for passive treatment of acid mine drainage with high Al and metal concentrations, Appl. Geochem. 23 (2008) 1660–1674.
[9] T.S. Rötting, J. Cama, C. Ayora, J.L. Cortina, J. de Pablo, Use of caustic magnesia to remove cadmium, nickel and cobalt from water in passive treatment systems: column experiments, Environ. Sci. Technol. 40 (2006) 6438–6443.
[10] J.L. Conca, J. Wright, Using an Apatite II^{TM} PRB to remediate groundwater contaminated with zinc, lead, and cadmium, in: The Remediation Technologies Development Forum Permeable Reactive Barriers Action Team Meeting, October 26–27, Best Western Winrock Inn Albuquerque, New Mexico, 2004.
[11] J.L. Conca, J. Wright, An Apatite II^{TM} permeable reactive barrier to remediate groundwater containing Zn, Pb and Cd, Appl. Geochem. 21 (2006) 2188–2200.
[12] Q.Y. Ma, T.J. Logan, S.J. Traina, Lead immobilization from aqueous solutions and contaminated soils using phosphate rocks, Environ. Sci. Technol. 29 (1995) 1118–1126.
[13] X. Chen, J.V. Wright, J.L. Conca, L.M. Peurrung, Evaluation of heavy metal remediation using mineral apatite, Water Air Soil Pollut. 98 (1997) 57–78.
[14] X. Cao, L.Q. Ma, D. Rhue, C.S. Appel, Mechanisms of lead, copper and zinc retention by phosphate rock, Environ. Pollut. 131 (2004) 435–444.
[15] A. Dybowska, D.A.C. Manning, M.J. Collins, T. Wess, S. Woodgate, E. Valsami-Jones, An evaluation of the reactivity of synthetic and natural apatites in the presence of aqueous metals, Sci. Total Environ. 407 (2009) 2953–2965.
[16] T. Suzuki, T. Hatsushira, Y. Hayakawa, Synthetic hydroxyapatites employed as inorganic cation-exchangers, J. Chem. Soc. Faraday Trans. I 77 (1981) 1059–1062.
[17] R. Liu, D. Zhao, In situ immobilization of Cu(II) in soils using a new class of iron phosphate nanoparticles, Chemosphere 68 (2007) 1867–1876.
[18] A. Corami, S. Mignardi, V. Ferrini, Cadmium removal from single- and multi-metal (Cd + Pb + Zn + Cu) solutions by sorption on hydroxyapatite, J. Colloid Interface Sci. 317 (2008) 402–408.
[19] A. Corami, F.D. Acapito, S. Mignardi, V. Ferrini, Removal of Cu from aqueous solutions by synthetic hydroxyapatite: EXAFS investigation, Mater. Sci. Eng. B 149 (2008) 209–213.
[20] W. Admassu, T. Breese, Feasibility of using natural fishbone apatite as a substitute for hydroxyapatite in remediating aqueous heavy metals, J. Hazard. Mater. B69 (1999) 187–196.
[21] J. Wright, K.R. Rice, B. Murphy, J.L. Conca, PIMS-remediation of Pb- contaminated soil at Camp Stanley, Texas, in: Proceedings of the Conference on Sustainable Range Management. ISBN: 1-57477-144-2, B4-04.
[22] S. Raicevic, J.V. Wright, V. Veljkovic, J.L. Conca, Theoretical stability assessment of uranyl phosphates and apatites: selection of amendments for in situ remediation of uranium, Sci. Total Environ. 355 (2006) 13–24.
[23] A. Corami, S. Mignardi, V. Ferrini, Copper and zinc decontamination from single- and binary-metal solutions using hydroxyapatite, J. Hazard. Mater. 146 (2007) 164–170.
[24] M. Sljivic, I. Smiciklas, I. Plecas, M. Mitric, The influence of equilibration conditions and hydroxyapatite physico-chemical properties onto retention of Cu^{2+} ions, Chem. Eng. J. 148 (2009) 80–88.
[25] Z. Elouear, J. Bouzid, N. Boujelben, M. Feki, F. Jamoussi, A. Montiel, Heavy metal removal from aqueous solutions by activated phosphate rock, J. Hazard. Mater. 156 (2008) 412–420.
[26] I. Smiciklas, A. Onjia, S. Raicevic, D. Janackovic, M. Mitric, Factors influencing the removal of divalent cations by hydroxyapatite, J. Hazard. Mater. 152 (2008) 876–884.
[27] S. Sugiyama, T. Ichii, M. Masayoshi, K. Kawashiro, Tomida, N. Shigemoto, H. Hayashi, Heavy metal immobilization in aqueous solution using calcium phosphate and calcium hydrogen phosphates, J. Colloid Interface Sci. 259 (2003) 408–410.
[28] E. Valsami-Jones, K.V. Ragnarsdottir, A. Putnis, D. Bosbach, A.J. Kemp, G. Cressey, The dissolution of apatite in the presence of aqueous metal cations at pH 2–7, Chem. Geol. 151 (1998) 215–233.
[29] J. Oliva, J. De Pablo, J.L. Cortina, J. Cama, C. Ayora, The use of Apatite II^{TM} to remove divalent metal ions zinc(II); lead(II); manganese(II) and iron(II) from water in passive treatment systems: column experiments, J. Hazard. Mater. 184 (2010) 364–374.
[30] S. Raicevic, T. Kaludjerovic-Radoicic, A.I. Zouboulis, In situ stabilization of toxic metals in polluted soils using phosphates: theoretical prediction and experimental verification, J. Hazard. Mater. B117 (2005) 41–53.
[31] J.J. Middelburg, R.N.J. Comans, Sorption of cadmium on hydroxyapatite, Chem. Geol. 90 (1991) 45–53.
[32] A. Yasukawa, T. Yokoyama, K. Kandori, T. Ishikawa, Reaction of calcium hydroxyapatite with Cd^{2+} and Pb^{2+} ions, Colloids Surf. A: Physicochem. Eng. Aspects 299 (2007) 203–208.
[33] J. Jeanjean, S. McGrellis, J.C. Rouchaud, M. Fedoroff, A. Rondeau, S. Perocheau, A. Bubis, A crystallographic study of the sorption of cadmium on calcium hydroxyapatites: incidence of cationic vacances, J. Solid State Chem. 126 (1996) 195–201.
[34] S. Mandjiny, K.A. Matis, A.I. Zouboulis, M. Fedoroff, J. Jeanjean, J.C. Rouchaud, N. Toulhoat, V. Potocek, C. Loos-Neskovic, P. Maireles-Torres, D. Jones, Calcium hydroxyapatites: evaluation of sorption properties for cadmium ions in aqueous solution, J. Mater. Sci. 33 (1998) 5433–5442.
[35] Q.Y. Ma, S.J. Traina, T.J. Logan, J.A. Ryan, Effects of aqueous Al, Cd, Cu, Fe(II), Ni, and Zn on Pb immobilization by hydroxyapatite, Environ. Sci. Technol. 28 (1994) 1219–1228.
[36] C.W. Cheung, C.K. Chan, J.F. Porter, G. McKay, Combined diffusion model for the sorption of cadmium, copper, and zinc ions onto bone char, Environ. Sci. Technol. 35 (2001) 1511–1522.

[37] W. Zheng, X. Li, F. Wang, Q. Yanga, P. Deng, G. Zeng, Adsorption removal of cadmium and copper from aqueous solution by areca—a food waste, J. Hazard. Mater. 157 (2008) 490–495.
[38] D.C.K. Ko, J.F. Poster, G. Mckay, Determination of solid-phase loading for the removal of metal ion from effluents using fixed-bed adsorbers, Environ. Sci. Technol. 35 (2001) 2797–2803.
[39] E. Mavropoulos, N.C.C. da Rocha, J.C. Moreira, L.C. Bertolino, A.M. Rossi, Pb^{2+}, Cu^{2+} and Cd^{2+} ions uptake by Brazilian phosphate rocks, J. Braz. Chem. Soc. 16 (2005) 62–68.
[40] W.D. Bostick, Use of Apatite for Chemical Stabilization of Subsurface Contaminants, Final Report, Work Performed under Contract: DE-AC26-01NT41306, US Department of Energy, 2003.
[41] J. Perrone, B. Fourest, E. Giffaut, Sorption of nickel on carbonate fluoroapatites, J. Colloid Interface Sci. 239 (2001) 303–313.
[42] Z. Elouear, R. Ben Amor, J. Bouzid, N. Boujelben, Use of phosphate rock for the removal of Ni^{2+} from aqueous solutions: kinetic and thermodynamics studies, J. Environ. Eng. ASCE 135 (2009) 259–265.
[43] I. Mobasherpour, E. Salahi, M. Pazouki, Removal of nickel (II) from aqueous solutions by using nano-crystalline calcium hydroxyapatite, J. Saudi Chem. Soc. 15 (2011) 105–112.
[44] A.G. Sowder, T. Khijniak, P.J. Morris, P.M. Bertsch, Evaluating the effect of apatite amendments on uranium and nickel toxicity in aged contaminant sediments, in: Paper # PB7-05, Presented at "Migration '99", Lake Tahoe, NV (UCRL-ID-13526), 1999.
[45] J. Gómez del Río, P.J. Morando, D.P. Cicerone, Natural materials for remediation of industrial effluents: comparative study of the retention of Cd, Zn and Co by calcite e HAP. Part I. Batch experiments, J. Environ. Manage. 71 (2004) 169–177.
[46] S. Dimovic, I. Smiciklas, I. Plecas, D. Antonovic, M. Mitric, Comparative study of differently treated animal bones for Co^{2+} removal, J. Hazard. Mater. 164 (2009) 279–287.
[47] X. Pan, J. Wang, D. Zhang, Sorption of cobalt to bone char: kinetics, competitive sorption and mechanism, Desalination 249 (2009) 609–614.
[48] I. Smiciklas, S. Dimovic, I. Plecas, M. Mitric, Removal of Co^{2+} from aqueous solutions by hydroxyapatite, Water Res. 40 (2006) 2267–2274.
[49] T.S.B. Narasaraju, D.E. Phebe, Some physico-chemical aspects of hydroxyapatite, J. Mater. Sci. 31 (1996) 1–21.
[50] I. Puigdomènech, Chemical Equilibrium Software Hydra and Medusa, Inorganic Chemistry Department, Technology Institute, Stockholm, Sweden, 2001.
[51] M. Peld, K. Tonsuaadu, V. Bender, Sorption and desorption of Cd^{2+} and Zn^{2+} ions in apatite-aqueous systems, Environ. Sci. Technol. 38 (2004) 5626–5631.
[52] I. Smiciklas, S. Milonjic, P. Pfendt, S. Raicevic, The point of zero charge and sorption of cadmium(II) and strontium(II) ions on synthetic hydroxyapatite, Sep. Purif. Technol. 18 (2000) 185–194.
[53] I. Smiciklas, A. Onjia, S. Raicevic, Experimental design approach in the synthesis of hydroxyapatite by neutralization method, Sep. Purif. Technol. 44 (2005) 97–102.
[54] Y. Xu, F.W. Schwartz, S.J. Traina, Sorption of Zn^{2+} and Cd^{2+} on hydroxyapatite surfaces, Environ. Sci. Technol. 28 (1994) 1472–1480.
[55] R. Zhu, R. Yu, J. Yao, D. Mao, C. Xing, D. Wang, Removal of Cd^{2+} from aqueous solutions by hydroxyapatite, Catal. Today 128 (2008) 94–99.
[56] Z. Zhang, M. Li, W. Chen, S. Zhu, N. Liu, L. Zhu, Immobilization of lead and cadmium from aqueous solution and contaminated sediment using nano-hydroxyapatite, Environ. Pollut. 158 (2010) 514–519.
[57] I.R. Sneddon, M. Orueetxebarria, M.E. Hodson, P.F. Schofield, E. Valsami-Jones, Use of bone meal amendments to immobilise Pb, Zn and Cd in soil: a leaching column study, Environ. Pollut. 144 (2006) 816–825.
[58] Y.-J. Wang, J.-H. Chen, Y.-X. Cui, S.-Q. Wang, D.-M. Zhou, Effects of low-molecular-weight organic acids on Cu(II) adsorption onto hydroxyapatite nanoparticles, J. Hazard. Mater. 162 (2009) 1135–1140.